

The mechanism of growth of the low-frequency East Asia–Pacific teleconnection and the triggering role of tropical intraseasonal oscillation

Jiabao Wang¹ · Zhiping Wen^{1,3,4} · Renguang Wu² · Yuanyuan Guo¹ · Zesheng Chen^{1,5}

Received: 10 March 2015 / Accepted: 24 August 2015 / Published online: 29 August 2015
© Springer-Verlag Berlin Heidelberg 2015

Abstract The East Asia–Pacific (EAP) pattern is a well-known meridional teleconnection over East Asia during boreal summer. In this study, the mechanism for growth of the EAP on intraseasonal timescale is investigated through a vorticity budget. It is found that the beta-effect and high-frequency transient eddies have primary contributions to the growth of the low-frequency EAP. The former leads to a westward shift of disturbances associated with the low-frequency EAP and the latter favors an amplification of disturbances, respectively. The interaction between low-frequency disturbances and zonal flow has a damping effect by dragging disturbances eastward. The impact of boreal summer intraseasonal oscillation (BSISO) on the triggering of the low-frequency EAP is also examined in this study based on observational analysis and a linear model experiment. It is shown that an elongated anomalous convection band located in the vicinity of Philippines associated with the dominant mode of BSISO has a significant impact on the initiation of low-frequency EAP via Rossby wave

propagation, whereas anomalous convection located over the North Indian Ocean has a limited impact. Based on the results of present study, the low-frequency EAP could be a self-sustained mode, and the BSISO plays a substantial role in triggering the low-frequency EAP.

Keywords Growth mechanism · Low-frequency EAP · ISO · Vorticity budget

1 Introduction

The East Asia–Pacific (EAP) teleconnection (Nitta 1987; Huang 1992) is a dominant mode of circulation anomalies over East Asia during boreal summer. It is a meridional pattern with tripole anomalous centers located over the South China Sea, North China and the Okhotsk Sea, respectively. A number of studies have been conducted to examine the mechanism of triggering and growth of the EAP pattern. They can be summarized as following five categories: (1) northward propagation of quasi-stationary planetary waves along East Asia initiated by heat source located around the Philippines or over the central Pacific at lower level (e.g., Nitta 1987; Huang 1992; Chen et al. 2014); (2) propagation of stationary Rossby waves along the Asian jet turning equatorward when reaching the East Asian coast at higher level (e.g., Enomoto et al. 2003; Hsu and Lin 2007); (3) propagation of barotropic Rossby wave train generated by typhoons (Kawamura and Ogasawara 2006; Yamada and Kawamura 2007); (4) a moist dynamical mode that sustains itself via dry energy conversion and interaction with moist processes (e.g., Kosaka and Nakamura 2006, 2008, 2010); (5) maintenance by subtropical precipitation anomalies which act as heat source (Lu and Lin 2009). Most of these previous studies focused primarily on interannual

✉ Zhiping Wen
eeswzp@mail.sysu.edu.cn

¹ Center for Monsoon and Environment Research and Department of Atmospheric Sciences, Sun Yat-sen University, Guangzhou 510275, China

² Center for Monsoon System Research, Institute of Atmospheric Physics, Chinese Academy of Sciences, Beijing 100029, China

³ State Key Laboratory of Severe Weather, Chinese Academy of Meteorological Sciences, Beijing, China

⁴ Jiangsu Collaborative Innovation Center for Climate Change, Nanjing, China

⁵ State Key Laboratory of Tropical Oceanography, South China Sea Institute of Oceanology, Chinese Academy of Sciences, Guangzhou, China

variations of the EAP pattern. The EAP, nevertheless, displays also variations on the intraseasonal timescale with peaks at 25–60 days (hereinafter low-frequency EAP; Wu et al. 2013). However, little attention has been paid to variations of the EAP on this timescale so far. Given that the EAP can exert significant impact on both regional and remote climate (Lau and Weng 2002; Hsu and Lin 2007; Choi et al. 2010; Kim et al. 2012; Li et al. 2014), a reexamination of mechanisms of growth and maintenance of the EAP, especially its intraseasonal component, is necessary, which is the main focus in this study. On the other hand, notwithstanding that a number of studies have demonstrated some crucial factors for maintaining the low-frequency anomalies in the midlatitudes (e.g., instabilities of the zonally asymmetric climatological flow, changes in quasi-stationary eddies and high-frequency transient eddy forcing, etc.; e.g., Hoskins and Karoly 1981; Egger and Schilling 1983; Simmons et al. 1983; Branstator 1984; Lau 1988; Nigam and Lindzen 1989; Kang 1990; Branstator 1990, 1992; Ting and Lau 1993), the exact role of different dynamic contributors in the growth of the low-frequency EAP remains unknown. Therefore, it is requisite to estimate particular contribution of each dynamical process quantitatively.

Tropical atmospheric intraseasonal oscillations (ISOs) are referred to as fluctuations with periods ranging from 10 to 90 days. On 30–90-day timescales, ISOs are mainly dominated by the Madden–Julian Oscillation (MJO; Madden and Julian 1971, 1972, 1994). On 10–20-day timescales, ISOs are dominated by convectively coupled Rossby and Kelvin waves (not addressed in this study). In the past few decades, increasing attention has been paid not only to the effect of MJO on tropical atmospheric and oceanic variability (e.g., McPhaden 1999, 2004, 2008; Zhang and Gottschalck 2002; Hendon et al. 2007; Seiki and Takayabu 2007; Rao et al. 2008; Hsu and Li 2011a, b; Duncan and Han 2012), but also to its influence on extratropical climate change and climate modes (e.g., Thompson and Wallace 2000; Straub and Kiladis 2003; Mori and Watanabe 2008; Lin et al. 2009; Johnson and Feldstein 2010; Deng and Jiang 2011; Yoo et al. 2012). A detailed review on the impact of MJO on weather and climate is offered by Zhang (2013).

The tropical–extratropical interaction has received much consideration in recent decades, especially the role of tropical anomalous convection associated with tropical ISO in extratropical climate modes. Schubert and Park (1991) first pointed out the possible phase locking between the Pacific–North American (PNA) pattern and the tropical convection in the western and central Pacific. This finding was reexamined by Mori and Watanabe (2008). They specifically showed that the positive (negative) phase of the PNA pattern is more likely to appear when anomalous convection

associated with MJO is inactive (active) over the region from the Bay of Bengal to the western Pacific. They further calculated the relative contribution of MJO in explaining the emergence of the PNA pattern. In a recent study, Lin et al. (2009) indicated a pronounced amplification of a positive (negative) phase of the NAO about 5–15 days after suppressed (enhanced) convection of the MJO enters the central Pacific, which is consistent with the numerical results of Cassou (2008). While considerable progresses have been made to delineate the coherence of MJO and extratropical climate modes during boreal winter, less effort has been made to explore the likely relationship between tropical ISO and extratropical climate modes (e.g., the EAP) during boreal summer. In light of inadequate endeavors made on above-mentioned aspect, it requires us to extend the work to boreal summer.

In the current study, we are particularly interested in the mechanism of growth of the low-frequency EAP. We use streamfunction tendency equation to obtain insight into the relative contributions of different internal dynamical processes in the growth of the low-frequency EAP quantitatively. The triggering effect of the ISO on the initial stage of the low-frequency EAP will also be evaluated by adopting a linear baroclinic model (LBM; Watanabe and Kimoto 2000). We have organized this article in the following sequence. Brief introductions to the data and model are provided in Sect. 2. The major characteristics of the low-frequency EAP are illustrated in Sect. 3. The mechanism of growth of the low-frequency EAP is discussed in Sect. 4. Section 5 shows triggering of the low-frequency EAP by ISO. The results are summarized in Sect. 6 along with discussion.

2 Data and model

2.1 Data

The following data spanning from 1979 to 2012 were used in this article: (1) daily averaged quantities derived from the global European Centre for Medium-Range Weather Forecasts (ECMWF) Interim reanalysis dataset (ERA-Interim; Dee et al. 2011). The variables include geopotential height, zonal wind and relative vorticity at 850, 500 and 200 hPa with horizontal resolution of 2.5° longitude \times 2.5° latitude; (2) National Oceanic and Atmospheric Administration (NOAA) interpolated outgoing longwave radiation (OLR) data as a proxy of anomalous convection associated with the ISO. In view of the EAP is dominant in boreal summer, this study focuses on the period of coverage from May to September.

For each given variable, slowly varying seasonal cycle was firstly defined by applying a 31-day running mean to

daily climatology. Then, the seasonal cycle was removed from raw daily data to generate daily anomaly. To anchor on the intraseasonal variability, the calendar mean for daily anomaly was further subtracted by which interannual variability was removed. At last, the Lanczos filter (Duchon 1979) was used to extract the low-frequency signal in the 30–60 day period and the high-frequency signal in the 2–8 day period.

2.2 Model

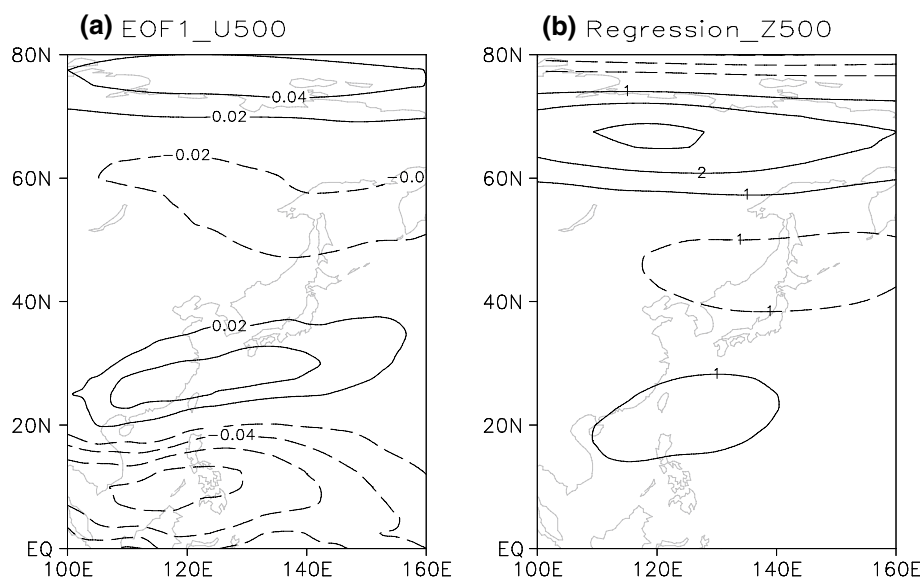
In this study, a LBM (Watanabe and Kimoto 2000, 2001) was utilized to examine the extratropical response to the heat source associated with the ISO. The primitive equations of LBM are identical to those in the atmospheric general circulation model (AGCM) developed at the Center for Climate System Research (CCSR), University of Tokyo, Japan and the National Institute for Environmental studies (NIES), but linearized by a basic state as observed boreal summer (May–September) climatology generated from ERA-Interim with the period coverage of 1979–2012. The model variables have a horizontal resolution of T42 and 20 unevenly spaced sigma levels in the vertical. Three dissipation terms are assigned as follows: damping timescale of 0.5 day for Biharmonic diffusion, damping timescale of 1 day applied only to the lower boundary layers and the uppermost two levels, leaving the rest with the timescale of 20 day, for Newtonian damping, and Rayleigh friction. We ran the model with time integration up to 30 days. Given that the time length for a tropic-forced poleward-propagation Rossby wave packet to reach high latitudes is about 10 days (Hoskins and Karoly 1981), an average from day 11 to day 15 was adopted to assess the direct and steady extratropical response to tropical forcing.

3 Major characteristics of the low-frequency EAP

In an attempt to examine the spatial pattern of the EAP, the empirical orthogonal function (EOF) analysis was applied to unfiltered and normalized 500-hPa zonal wind anomalies over 100°E–160°E, 0°–80°N. The leading EOF mode is characterized by four evident anomalous centers with alternating signs (Fig. 1a). According to the meridional shear of zonal wind, a meridional tripole structure with two anticyclonic anomalies centered over the Philippines and East Russia and one cyclonic anomaly located over Japan is considered as the canonical positive phase of the EAP (Huang and Li 1987). Indeed, a tripole pattern as identified by previous studies can be readily seen in Fig. 1b that is obtained by regression of the 500-hPa geopotential height field upon the first principal component (PC1). This suggests that the EAP is a dominant mode of teleconnection over East Asia during boreal summer.

To further detect the predominant period of the EAP, power spectral analysis was conducted on PC1. The spectral analysis has been applied to PC1 which is separated into 34 segments to represent 34 years (1979–2012), and then an average of the analysis results across all 34 years is displayed in Fig. 2. The prevailing periods of the EAP stand out with peaks at 30–60 day period (consistent with Wu et al. 2013) and 10–20 day period (not concerned in this study) with statistical significance exceeding the 90 % level. This means that the EAP appears to be dominated by intraseasonal variation. The correlation coefficient between 30 and 60 day band-pass filtered PC1 with raw PC1 is 0.66, and the former could explain up to 38 % of the total variance. This further confirms the finding that the EAP fluctuates primarily on intraseasonal timescale. After reapplying the EOF to 30–60 day filtered and normalized 500-hPa

Fig. 1 **a** Spatial pattern of EOF1 of the unfiltered daily 500-hPa zonal wind anomalies. **b** The 500-hPa geopotential height anomalies regressed onto the PC1 associated with **(a)**. The contour interval is 1 m



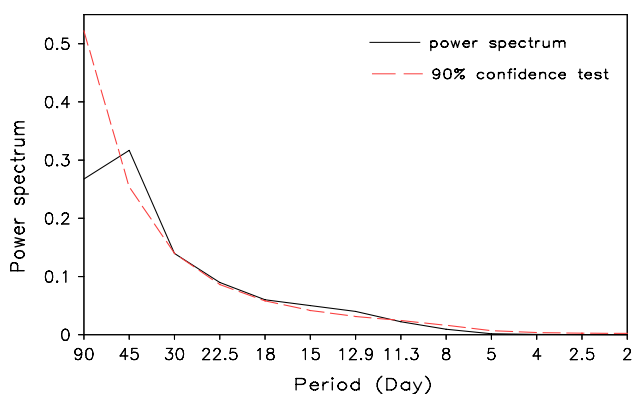


Fig. 2 34 years-mean (1979–2012) power spectrum of PC1 (solid black line). Also shown is the 90 % confidence upper limits of red noise spectrum (dashed red line)

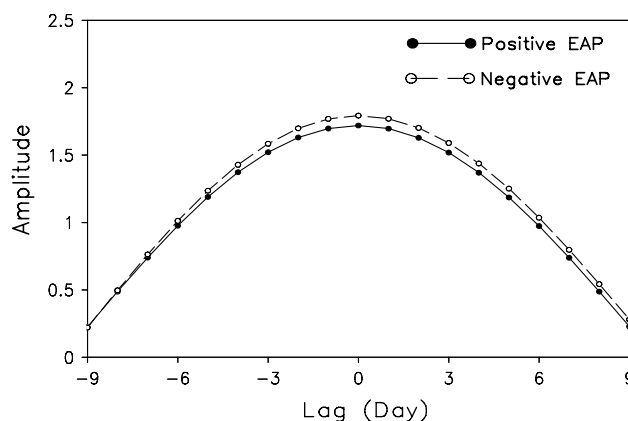


Fig. 4 Lagged composite time evolution of PC1 associated with the leading EOF mode of filtered 500-hPa geopotential height anomalies. The positive (negative) phase of the low-frequency EAP is indicated by solid (dashed) line with solid (hollow) circles. The sign of the negative phase has been flipped after conducting lag composite analysis

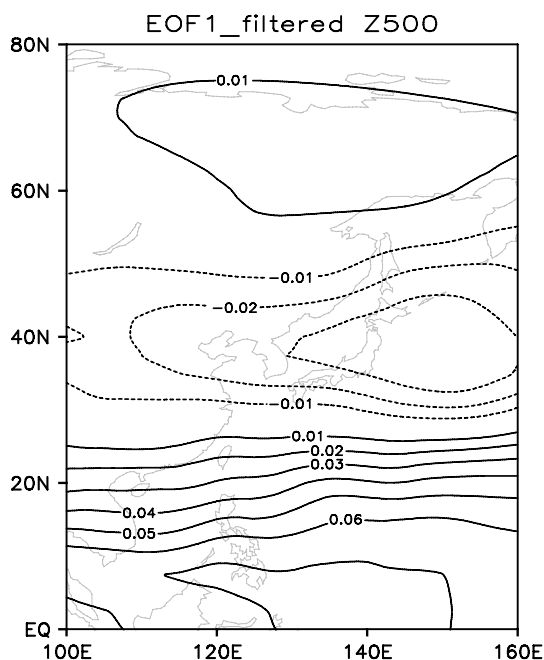


Fig. 3 Spatial pattern of the leading mode of the low-frequency filtered daily 500-hPa geopotential height anomalies

geopotential height anomalies (Fig. 3), the result yields a well-organized tripole pattern almost identical to the unfiltered one with percent variance of approximately 18 %.

Spatial distribution and dominant period of the low-frequency EAP (referred to as the EAP in the rest of this article for brevity) have so far been clearly described hereinbefore. The temporal evolution of the EAP will then be discussed in the rest of this section. During the entire length of the normalized PC1 corresponding to the leading mode of filtered 500-hPa geopotential height field, 89 (91) positive (negative) intact EAP events have been identified, among which only 50 (46) positive (negative) typical events

are extracted to perform the composite analysis based on the following criteria. First, the chosen EAP events must be typical and persistent. In other words, the normalized PC1 needs to exceed one standard deviation and prolong for at least 5 days. Second, an event that has successive peaks without transition to the opposite phase is discarded. Before performing composite analysis to the spatial field, the average persistent period of positive (negative) EAP events is first determined by applying composite analysis to the normalized PC1. As shown in Fig. 4, the positive (negative) EAP persists approximately 19 days and two phases bear symmetry. Mori and Watanabe (2008) exhibited the same feature for the low-frequency PNA, which suggests that some of the extratropical climate modes share some common features.

Lagged composite anomalies of the low-frequency 500-hPa geopotential height for the positive EAP events are presented in Fig. 5. The wave-activity flux (WAF) defined by Takaya and Nakamura (2001) was used to represent the energy propagation of Rossby wave-like perturbation in the quasi-geostrophic framework that is indicated by arrows in the figure. This flux is independent of wave phase and parallel to the local group velocity of Rossby waves. A number of studies have used this powerful diagnostic tool to identify the energy propagation of the observed perturbation (e.g., Hsu and Lin 2007). Note that at the initial stage of the positive EAP, significant anomalies emerge over the North Pacific with three obvious centers (Fig. 5a). At day -6, the northern positive anomaly extends northwestward and the southern two negative anomalies move westward with an evident intensification (Fig. 5b). As time progresses, the northern positive anomaly keeps shifting westward slowly and the southern two negative anomalies merge together with slight westward movement and result in a zonally

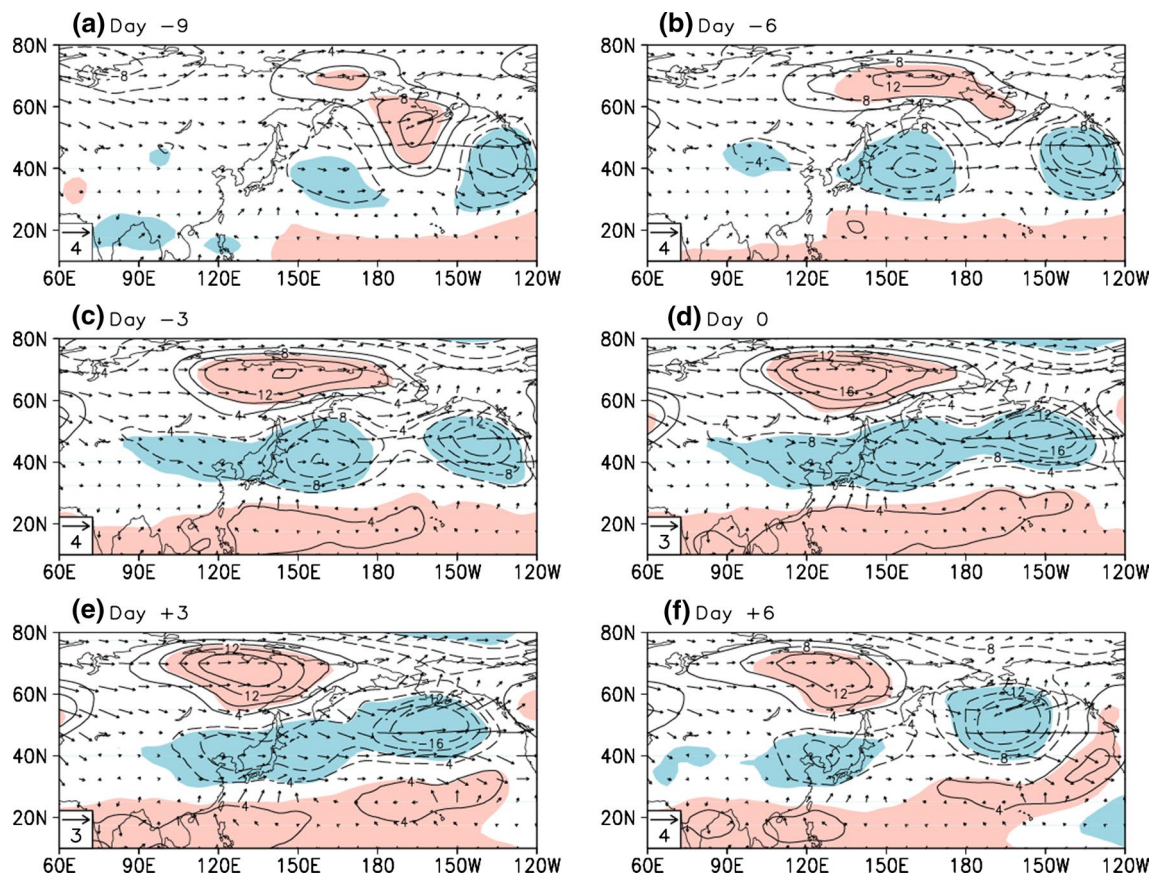


Fig. 5 Maps of lagged composite 500-hPa geopotential height anomalies (contour, unit: m) and wave-activity flux (vector, unit: $\text{m}^2 \text{s}^{-2}$) in respect of selected typical positive low-frequency EAP events. The regions with the t -value exceeding the 95 % confidence level are shaded

extended band across the entire North Pacific. At the meantime, a positive anomaly center appears at day -3 in tropics and develops into the low latitude center of the EAP eventually (Fig. 5c). At the peak day, a well-organized tripole pattern can be found over East Asia with a zonally extended structure, which resembles the classical EAP (Fig. 5d). After that, the middle latitude center weakens rapidly and breaks apart at day $+6$, while the low latitude center breaks apart without weakening and the high latitude center decays slowly. The temporal evolution of the negative EAP events is nearly the same as the positive ones, merely with opposite signs (figure not shown). Note that the direction of wave energy propagation along the East Asia is poleward at this level, indicating the role of tropical heating in the growth of the positive low-frequency EAP as mentioned in earlier studies (e.g., Nitta 1987; Huang 1992; Hsu and Lin 2007). Another persistent wave activity can be identified in the mid-latitudes and high latitudes, which travels eastward across the Eurasian continent and the North Pacific.

The main features are largely similar at different levels. Nevertheless, there still exist some distinctions (figures not shown). A poleward propagation of wave activity along the

East Asian coast at 850 and 500 hPa is replaced by an equatorward-propagating wave activity at 200 hPa. At 850 hPa, the energy propagation is rather weak over the Eurasian continent without specific direction, while it is obvious in the middle and upper troposphere.

It is worth mentioning here that the composite results are partially different from the features documented by Wu et al. (2013). For instance, the eastward energy propagation over the Eurasian continent is invisible at 500 hPa and the zonally extended structure of the EAP is absent as well in their study. These discrepancies could be attributed to different levels of zonal winds for the EOF analysis conducted to extract the EAP. In this study, the EOF analysis was performed on 500-hPa zonal winds, while in Wu et al. (2013) on 850-hPa zonal winds. In this sense, there would be more low-latitude signals in Wu et al. (2013).

4 The mechanism of growth of the EAP

The temporal evolution presented above reveals pronounced westward movement and intensification during the

growth period of the EAP. To clarify relative roles of various dynamical processes in the growth of the EAP, a vorticity budget analysis is conducted in this section using the low-frequency streamfunction (ψ_L) tendency equation (Cai and van den Dool 1994; Feldstein 1998, 2002), which can be written as:

$$\frac{\partial \psi_L}{\partial t} = \sum_{i=1}^7 \xi_i + R, \quad (1)$$

where

$$\xi_1 = \nabla^{-2} \left\{ - \left(v_r^L + v_d^L \right) \frac{1}{a} \frac{df}{d\theta} \right\},$$

$$\xi_2 = \nabla^{-2} \left(- [\overline{\mathbf{V}_r}] \cdot \nabla \zeta^L - \mathbf{V}_r^L \cdot \nabla [\overline{\zeta}] \right) + \nabla^{-2} \left(- [\overline{\mathbf{V}_d}] \cdot \nabla \zeta^L - \mathbf{V}_d^L \cdot \nabla [\overline{\zeta}] \right),$$

$$\xi_3 = \nabla^{-2} \left(- \overline{\mathbf{V}_r^*} \cdot \nabla \zeta^L - \mathbf{V}_r^L \cdot \nabla \overline{\zeta^*} \right) + \nabla^{-2} \left(- \overline{\mathbf{V}_d^*} \cdot \nabla \zeta^L - \mathbf{V}_d^L \cdot \nabla \overline{\zeta^*} \right),$$

$$\xi_4 = \nabla^{-2} \left(- (f + \overline{\zeta}) \nabla \cdot \mathbf{V}_d^L - \zeta^L \nabla \cdot \overline{\mathbf{V}_d} \right),$$

$$\xi_5 = \nabla^{-2} \left(- \mathbf{V}_r^L \cdot \nabla \zeta^L \right)^L + \nabla^{-2} \left\{ - \nabla \cdot \left(\mathbf{V}_d^L \zeta^L \right) \right\}^L,$$

$$\xi_6 = \nabla^{-2} \left(- \mathbf{V}_r^H \cdot \nabla \zeta^H \right)^L + \nabla^{-2} \left\{ - \nabla \cdot \left(\mathbf{V}_d^H \zeta^H \right) \right\}^L,$$

$$\xi_7 = \nabla^{-2} \left(- \mathbf{V}_r^L \cdot \nabla \zeta^H \right)^L + \nabla^{-2} \left\{ - \nabla \cdot \left(\mathbf{V}_d^L \zeta^H \right) \right\}^L + \nabla^{-2} \left(- \mathbf{V}_r^H \cdot \nabla \zeta^L \right)^L + \nabla^{-2} \left\{ - \nabla \cdot \left(\mathbf{V}_d^H \zeta^L \right) \right\}^L,$$

and ψ is the stream function, v the meridional wind component, a the earth's radius, f the Coriolis parameter, \mathbf{V} the horizontal wind vector, and ζ the relative vorticity. The term R designates a residual which consists of physical processes that have been neglected such as dissipation, external forcing, and tilting terms. The subscripts "r" and "d" denote the rotational and divergent components of the horizontal wind, respectively, and the superscripts "L" and "H" represent low-frequency and high-frequency quantities, respectively. For a given variable, an overbar indicates a time mean, a square bracket a zonal mean, and an asterisk a deviation from the zonal mean. The low-frequency streamfunction tendency $\frac{\partial \psi_L}{\partial t}$ which is calculated using central difference thus can be measured by the summation of (1) beta effect, (2) interaction between low-frequency

anomalies and zonal symmetric (asymmetric) daily-mean flow, (3) divergence, (4) self-interaction among low-(high-) frequency anomalies, and (5) cross-scale interactions as shown from ξ_1 to ξ_7 respectively in the equation above. The first four terms on the right-hand side (rhs) are linear terms, while the other three denote nonlinear processes. In practice, dynamical mechanism of the growth of the EAP can be diagnostically determined by evaluating the relevant contributions of terms in Eq. (1).

In order to understand the mechanism of growth of the EAP, composite analysis was conducted for each term in Eq. (1) following the same procedure as mentioned in Sect. 3. To explicitly show the contribution of each term on the rhs (neglecting the residual) to the growth of the EAP, every composite field was then projected onto the spatial pattern at peak day of the composite 500-hPa streamfunction anomalies for each phase of the EAP (same method as Feldstein 2002). The domain chosen for projection is 60°E–120°W, 0°–80°N. The time series of the projection result are shown in Fig. 6. For brevity, only the result of positive phase is shown.

It can be clearly seen that the low-frequency streamfunction tendency term ($\frac{\partial \psi_L}{\partial t}$) and the summation of seven contribution terms (total) matches well during entire composite period (Fig. 6a). This suggests that it is appropriate to use Eq. (1) in detecting the role of internal dynamic processes in the growth of the EAP. A comparison of the sum of linear terms and that of nonlinear terms with the total indicates that the influence of linear terms on changes of $\frac{\partial \psi_L}{\partial t}$ overrides the impact of nonlinear terms (Fig. 6b). A closer observation into the projection coefficient of each linear term (Fig. 6c) demonstrates that ξ_1 favors both the growth and the decay of the EAP and nearly varies at the same pace with $\frac{\partial \psi_L}{\partial t}$. By contrast, ξ_2 and ξ_3 act to damp the growth and the decay of the EAP. The divergent term ξ_4 remains close to zero at the initial stage of the EAP, but jumps above zero after the establishment of the EAP and sustains a positive value thereafter. With this feature in mind, we propose that ξ_4 is a response to the establishment of the EAP instead of a forcing term. As shown above, the first three linear terms (ξ_1 , ξ_2 , ξ_3) cast substantial contributions to the growth and the decay of the EAP. On the other hand, further examination of the nonlinear terms (Fig. 6d) reveals a relatively important role of high-frequency transient eddies in the growth of the EAP, which is consistent with previous studies (e.g., Egger and Schilling 1983; Lau 1988; Black and Dole 1993; Jin et al. 2006a, b).

As a comparison, the time series of the projection coefficient of the negative phase (figures not shown) display features almost in accordance with the positive phase with several exceptions. First, the effect of the sum of all dynamic processes on the rhs of Eq. (1), $\sum_{i=1}^7 \xi_i$, is overstated in

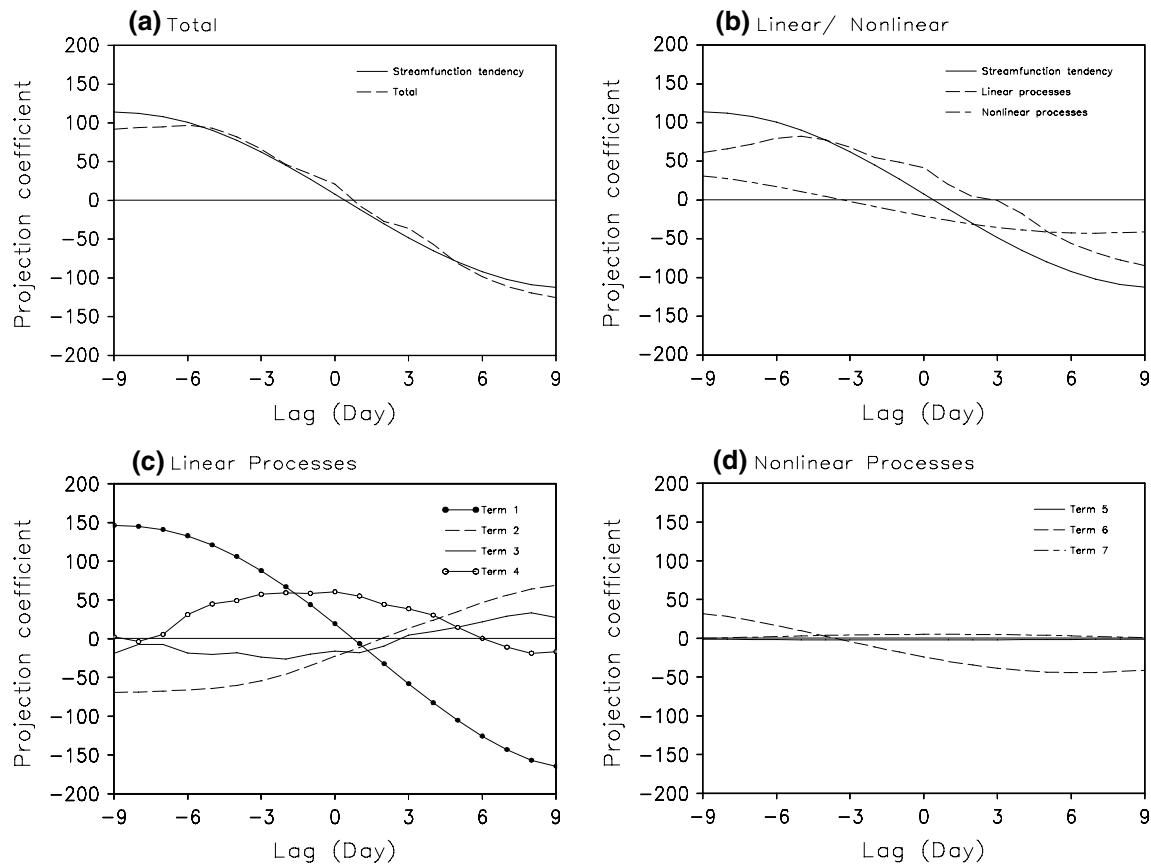


Fig. 6 Time series of various combinations of terms on the *rhs* of Eq. (1) projected onto the composite peak-day 500-hPa streamfunction anomalies for the positive phase of the low-frequency EAP. The terms being projected are **a** $\frac{\partial \psi_L}{\partial t}$ and $\sum_{i=1}^7 \xi_i$; **b** $\frac{\partial \psi_L}{\partial t}$, $\sum_{i=1}^4 \xi_i$ and

$\sum_{i=5}^7 \xi_i$; **c** four linear terms: ξ_1 to ξ_4 ; **d** three nonlinear terms: ξ_5 to ξ_7 . The specific indicator for *each line* has already been shown at the *top right corner in each plot*

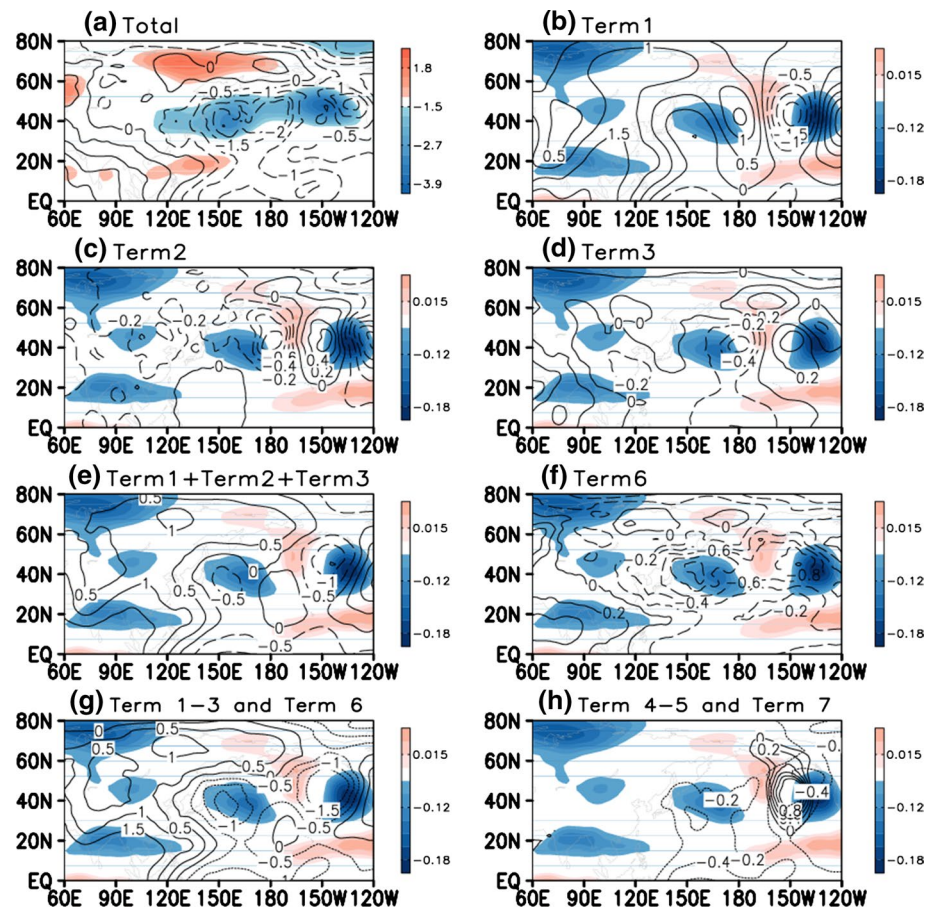
the growth of the negative phase of the EAP since its value is almost twice as large as the value of $\frac{\partial \psi_L}{\partial t}$. This kind of biased estimate should be attributed to the drawbacks of the projection technique (Feldstein 2002). Second, the divergent term ξ_4 plays a much more important role in the initial stage of the negative phase of the EAP. This asymmetry of the role of ξ_4 in different polarity of the EAP is intriguing and needs further investigation. In spite of differences in details above, the overall feature of the two polarities of the EAP is the same. The results imply a critical role of the beta effect in both the growth and the decay of the EAP, a positive contribution of the high-frequency transient eddies, and a prohibiting effect of the interaction between low-frequency anomalies and zonal symmetric (asymmetric) daily-mean flow.

Considering that the projection procedure can only diagnose which terms on the *rhs* of Eq. (1) account for changes of $\frac{\partial \psi_L}{\partial t}$, but fail to distinguish the exact way by which those terms act to influence its changes (Feldstein 1998), it is requisite to perform a pattern comparison thereafter (Fig. 7). In light of the largest growth rate of the EAP at day -9

(Fig. 6a), only the result of that day is presented. The pattern comparison of the negative phase of the EAP is also omitted. As shown in Fig. 7a, the spatial structure of $\frac{\partial \psi_L}{\partial t}$ is similar to that of $\sum_{i=1}^7 \xi_i$ considerably, with two positive anomalies located over the South China Sea and East Russia and one negative anomaly band across the North Pacific. This further supports the appropriate utilization of Eq. (1) in detecting the mechanism of growth of the EAP and the importance of internal dynamic processes for its growth.

Composite pictures of three linear terms (ξ_1 , ξ_2 , ξ_3) are illustrated in Figs. 7b–d, respectively. In these pictures and the following ones, the shading represents ψ_L rather than $\frac{\partial \psi_L}{\partial t}$ for the sake of exploring the way in which each dynamic term affects the growth of the EAP. If we compare the locations of anomalous centers of ξ_1 with those of the corresponding observed composite ψ_L (Fig. 7b), the phase difference indicates that the beta effect tends to favor the westward movement of existing disturbances over the North Pacific. By the same token, ξ_2 and ξ_3 serve as shifting the disturbances eastward (Fig. 7c, d), which

Fig. 7 Spatial distributions of various combinations of terms on the *rhs* of Eq. (1) at day -9 for the positive phase of the low-frequency EAP. The contour represents **a** $\sum_{i=1}^7 \xi_i$, **b** ξ_1 , **c** ξ_2 , **d** ξ_3 , **e** $\sum_{i=1}^3 \xi_i$, **f** ξ_6 , **g** sum of $\sum_{i=1}^3 \xi_i$ and ξ_6 , **h** sum of ξ_4 , ξ_5 and ξ_7 , respectively. The contour interval of **a**, **b**, **e**, **g** is $0.5 \times 10^6 \text{ m}^2 \text{ s}^{-2}$ while of **c**, **d**, **f**, **h** is $0.2 \times 10^6 \text{ m}^2 \text{ s}^{-2}$. The shading indicates the spatial pattern of the *lhs* of Eq. (1) in **a** with the interval of $0.3 \times 10^6 \text{ m}^2 \text{ s}^{-2}$ while denotes streamfunction anomalies in **b–h** with the interval of $0.015 \times 10^6 \text{ m}^2 \text{ s}^{-1}$



might damp the observed westward movement of disturbances during their growth period and result in negative contribution to the growth of the EAP. The total effect of the summation of ξ_1 , ξ_2 , ξ_3 is estimated in Fig. 7e. The result shows that although the beta effect term (ξ_1) is partially offset by linear interaction terms (ξ_2 and ξ_3), they together cause the westward movement of the positive EAP. As for ξ_6 , although its effect is relatively small, it helps the existing disturbances evolve to the canonical EAP by amplifying the negative anomalies and weakening the positive anomalies over the North Pacific and, meanwhile, strengthening the positive anomalies over the eastern Russia and damping the negative anomalies over the South China Sea. To further illustrate that the effect of ξ_1 , ξ_2 , ξ_3 and ξ_6 on the growth of the EAP overrides the rest terms of Eq. (1), the summation of ξ_1 , ξ_2 , ξ_3 and ξ_6 is displayed in Fig. 7g along with the summation of ξ_4 , ξ_5 and ξ_7 (Fig. 7h). It could be readily seen that the values and spatial pattern of sum of Terms 1–3 and Term 6 bear considerable similarity with $\sum_{i=1}^7 \xi_i$ (contours in Fig. 7a). This indicates that Terms 1–3, together with the Term 6, make major contributions to the evolution of the EAP. However, the values of the sum of Terms 4–5 and Term 7 are much smaller than $\sum_{i=1}^7 \xi_i$, which suggests a limited

role of Terms 4–5 and Term 7 in the development of the EAP.

Through above discussion, a short summary is given accordingly. First, the beta effect is crucial for the growth of the positive EAP. It drives the westward movement of the EAP and hence favors its development into the mature phase. Second, interaction between the low-frequency anomalies and zonal symmetric (asymmetric) climatologic flow acts to damp the westward movement of the EAP by shifting the disturbances associated with the EAP eastward. Last, high-frequency transient eddies play an important role in intensifying the evolution of the EAP, albeit with small amplitude. The relative role of each dynamic process in the growth of the EAP has been examined so far. However, why those processes influence the EAP in those ways remains unknown, further research will be needed to address this problem in future study.

5 The impact of ISO on the triggering of the EAP

In this section, special attention is given to the triggering of the EAP. In light of the fact that the low-frequency streamfunction tendency discussed in Sect. 4 cannot be

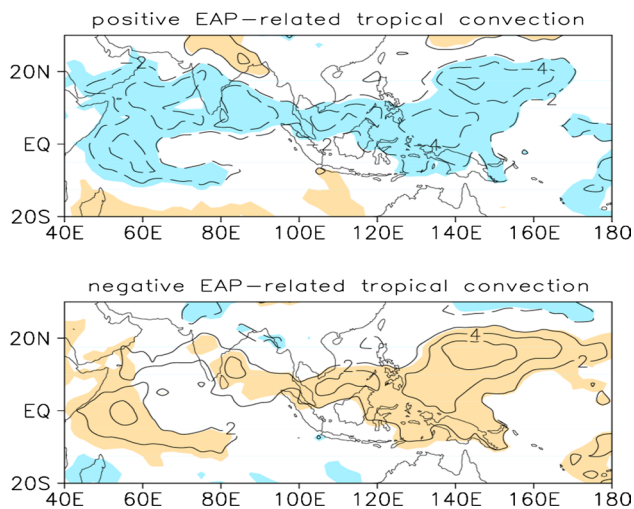


Fig. 8 Spatial pattern of low-frequency OLR anomalies averaged from 11 to 15 days before the day -9 of (top) positive, (bottom) negative phase of the EAP. The contour interval is 2 W m^{-2} (zero contour is omitted). Significant values exceeding the 99 % confidence level according to the Student t test are shaded

fully explained by the summation of dynamic processes at the initial stage of the positive EAP (Fig. 6a), external forcing, e.g., tropical convection, would be investigated in the remainder of this article. In this study, we mainly focused on the tropical convection associated with the ISO.

To investigate the possible impact of the ISO on the triggering of the EAP, we first extract the EAP-related ISO by applying lagged composite analysis to the low-pass filtered OLR anomalies over $40^{\circ}\text{E}–180^{\circ}$, $20^{\circ}\text{S}–30^{\circ}\text{N}$ according to the evolution of the EAP. Considering that the response time of extratropical circulation to the heating source in the tropics is over 10 days, the lead time was chosen from 11 to 15 days to derive corresponding composite results. Since the main focus of this section is the triggering effect of the ISO on the EAP, only the composite result of OLR anomalies before the day -9 of positive and negative phases of the EAP is presented. As shown in Fig. 8, distribution of anomalous low-frequency tropical convection prior to the emergence of extratropical circulation associated with the positive (negative) EAP is characterized by salient elongated negative (positive) anomalies over the North Indian Ocean and the western Pacific. This result leads us to speculate that, at the initial stage, tropical convective anomalies associated with the ISO might have a vital triggering impact on the EAP.

To test the hypothesis that tropical convection associated with the ISO might play a critical role in the triggering of the EAP, a forced numerical experiment with the LBM described in Sect. 2 was carried out. It needs to be mentioned here that although the convective anomaly

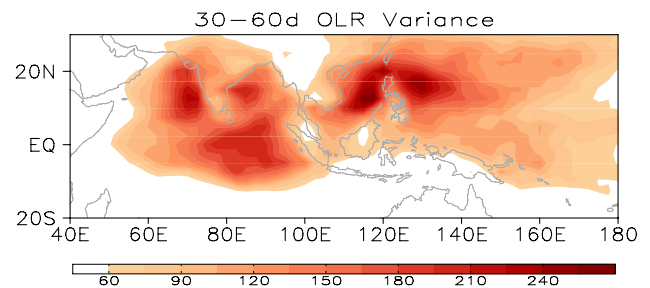


Fig. 9 Spatial distribution of variance of summer low-frequency OLR anomalies. Values above $60 \text{ W}^2 \text{ m}^{-4}$ are shaded

located over the western Pacific and that over the northern Indian Ocean merge together (Fig. 8), we still regard them as two different convective centers in terms of their propagating direction (figure not shown) and the distribution of filtered OLR variance (Fig. 9). Two maximum variance regions are located in the northern Indian Ocean ($60^{\circ}\text{E}–90^{\circ}\text{E}$, $5^{\circ}\text{N}–20^{\circ}\text{N}$) and in the vicinity of Philippines ($110^{\circ}\text{E}–140^{\circ}\text{E}$, $5^{\circ}\text{N}–20^{\circ}\text{N}$), respectively. What's more, in light of the numerical model used in this study is a linear model, only the result of extratropical circulation in response to the heat sources located over the tropics would be shown.

On the basis of the spatial pattern of anomalous tropical convection and the distribution of summer filtered OLR variance, three numerical experiments were conducted in this study. In the first experiment, two elliptic heat sources centered separately at 130°E , 13°N and 75°E , 10°N with the maximum heating rate centered at 400 hPa were imposed to investigate the joint impact of anomalous heating over the North Indian Ocean and that over the western Pacific on the triggering of the positive EAP. In the second experiment, only one elliptic heat source centered at 75°E , 10°N was imposed to analyze the sole impact of anomalous heating over the northern Indian Ocean on the initiation of the positive EAP. The heat source imposed in the second experiment was substituted by a heat source centered at 130°E , 13°N to ascertain the individual influence of tropical convection over the western Pacific on the triggering of the positive EAP in the third experiment. In light of our aims at understanding the general process of extratropical response, imposing the exact shape and exact intensity of the heat source is not essential to this simulation. Besides, it is acknowledged that the following results present an idealized scenario that only qualitatively illustrates the possible impact of heating on the triggering of the EAP.

Figure 10 illustrates the model response of 500-hPa geopotential height along with the observational result. Three alternating positive and negative anomaly centers could clearly be seen over the northern Pacific in response to the

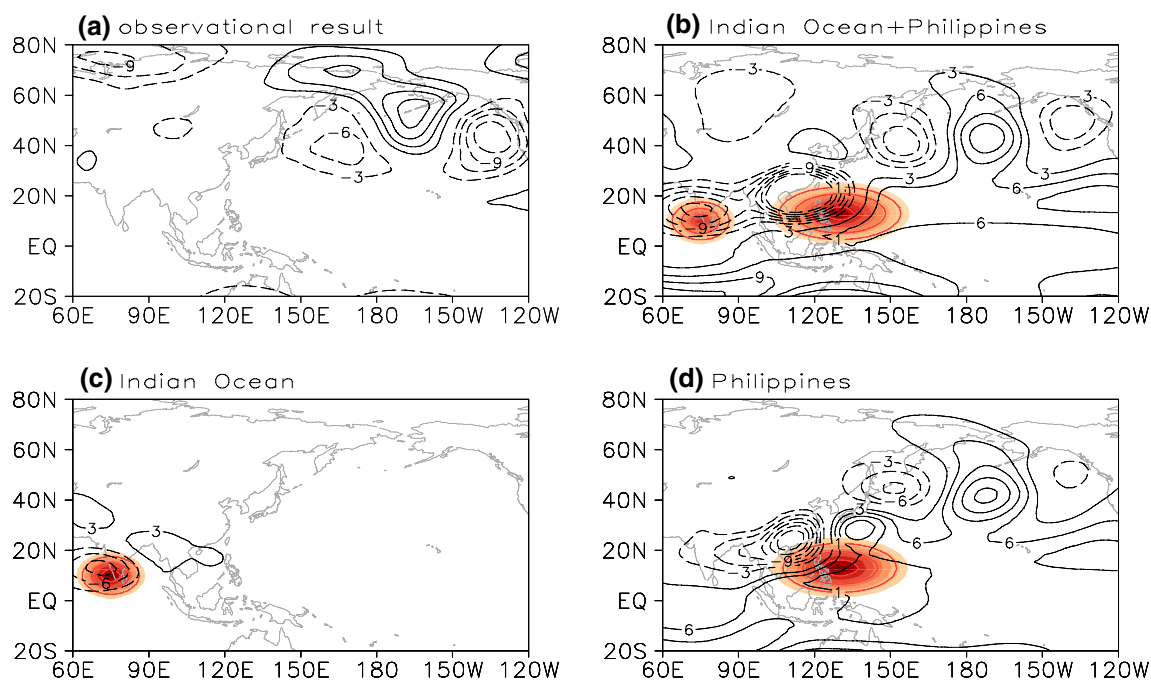


Fig. 10 **a** Observational composite spatial pattern of 500-hPa geopotential height anomalies (contour in *black*, unit: m) in respect of the day -9 of positive phase of the EAP. Averaged 500-hPa geopotential height anomalies from 11 to 15 days (contour in *black*, unit: m) in response to the imposed heat source (*shading*) over **b** the western

Pacific and the North Indian Ocean, **c** the North Indian Ocean only, **d** the western Pacific only. The *red ellipses* represent the horizontal distribution of heat sources at 0.45 sigma level (interval: 1 K/day). Zero contour is omitted in *both panels*

anomalous heating over the western Pacific and the North Indian Ocean (Fig. 10b), which is broadly identical to the observation (Fig. 10a). The above result lends confidence to our previous presumption that anomalous tropical convection associated with the ISO casts substantial effect on the triggering of the EAP. When examining relative roles of anomalous tropical convection located over the western Pacific and that over the northern Indian Ocean in detail, the joint influence on the initiation of the positive EAP should be attributed only to the anomalous convection over the western Pacific since anomalous heating imposed in the Indian Ocean has nearly no effect on it (Fig. 10c, d).

The above results pointed out the pivotal role of the ISO in triggering different polarities of the EAP from perspective of EAP-related ISO. To test whether the EAP-related ISO represents the dominant mode of boreal summer ISO (BSISO, defined by Kikuchi et al. (2012)), an extended EOF (EEOF) analysis was applied to the low-frequency filtered OLR data over $40^{\circ}\text{E}-180^{\circ}$, $20^{\circ}\text{S}-30^{\circ}\text{N}$. The EEOF analysis could better capture the northward movement of the BSISO mode than the EOF analysis used in Wheeler and Hendon (2004). The lag time chosen in this study is 5 days according to the dominant period of the ISO. The first two leading modes (EEOF1 and EEOF2), combined together, account for approximately 25 % of the total variance. However, since they have no triggering impact on the

EAP based on our research (not shown), our main focus will then turn to the next two modes (EEOF 3 and EEOF 4). EEOF 3 and EEOF 4 explains about 7.54 and 6.42 % of the total variance, respectively, which is separable from other modes based on the criterion of North et al. (1982). As expected, this pair of EEOFs represent a half cycle of the BSISO (Fig. 11), which is characterized by a pronounced northward movement over the northern Indian Ocean and a predominant northwestward propagation over the western Pacific. As a consequence, an elongated convective band tilting from southwest to northeast is apparent over the entire region mentioned above. A comparison between the structure of the EEOF3 and EEOF4 with that of EEOF1 and EEOF2 yields several striking differences: (1) convective anomalies located over the tropical Indian Ocean and those over the northwestern Pacific are of the same sign in EEOF3 and EEOF4 but opposite signs in EEOF1 and EEOF2; (2) the convective band in EEOF3 and EEOF4 tilts from southwest to northeast instead of tilting from northwest to southeast as in EEOF1 and EEOF2. However, the main feature of the EEOF3 and EEOF4 that main convective anomalies located over the northwestern Pacific and the North Indian Ocean tend to vary in phase bears considerable similarity with the EAP-related ISO. In this sense, the EAP-related ISO is considered as a dominant mode over the western Pacific and Indian Ocean though it is not the leading mode.

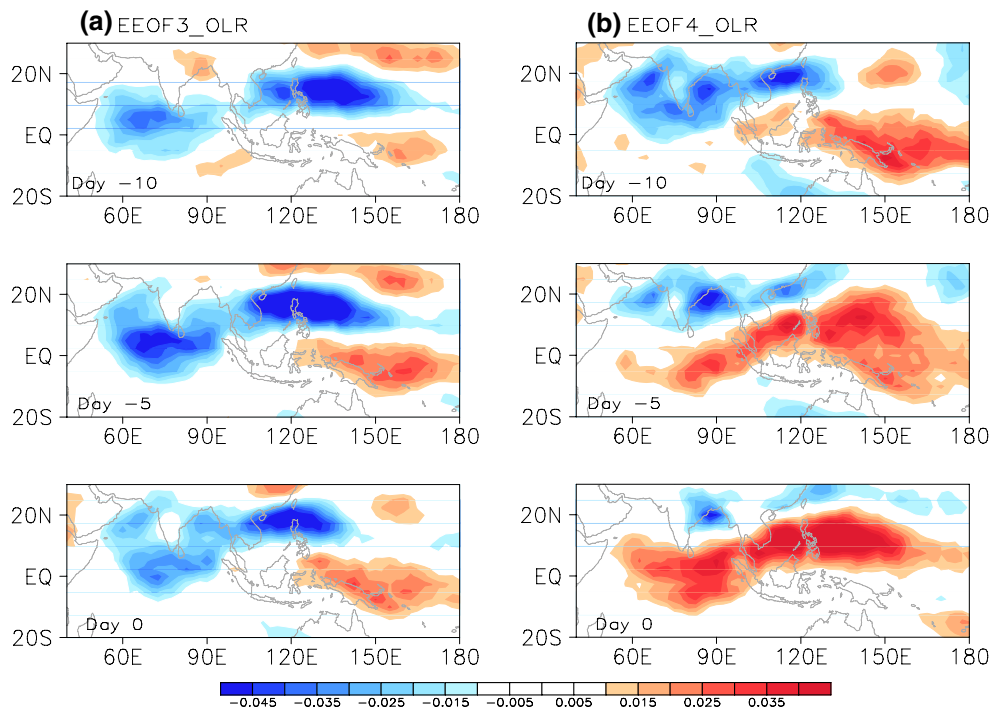


Fig. 11 Spatial–temporal pattern of the third (a) and the fourth (b) extended EOF mode of low-frequency OLR anomalies associated with intraseasonal oscillation during boreal summer (May–September,

referred to as BSISO) for the period 1979–2012. The combined two modes presented above indicate a half cycle of the BSISO

6 Summary and discussion

East Asia–Pacific (EAP) teleconnection, a dominant intraseasonal mode over East Asia with peaks at 30–60 day period, is characterized by a salient westward movement and amplification during its growth. In present study, the mechanism for the growth of the EAP and triggering by the BSISO are investigated by means of diagnostic analysis and numerical experiments. The findings documented in this article not only provide us with a better understanding of the mechanism for the growth of the EAP, but also give guidance for effort to forecast the initiation of the EAP according to its link with the BSISO.

According to the results of vorticity budget analysis (presented in Sect. 4), the growth of the EAP is primarily governed by linear dynamical processes. Specifically, the beta effect drives its growth by favoring its westward movement, while the interaction between the basic flow and low-frequency disturbances acts to damp its growth via shifting it eastward. Among nonlinear processes, high-transient eddies play a relatively important role in the intensification of the EAP. In contrast, other nonlinear processes, namely interaction between low-frequency anomalies and cross-scale interaction, have very limited impact on its growth.

Since dynamical processes cannot explain the initiation of the EAP completely, the role of tropical convection related

to the ISO is examined in the remainder of our study (displayed in Sect. 5). From perspective of the EAP-related ISO, convective anomalies in the vicinity of Philippines precede the initiation of the positive EAP by about 10 days, which suggests the possible triggering effect of tropical convection associated with the ISO on the EAP. This observational result is further demonstrated with the aid of LBM, in which heat sources were imposed to mimic the tropical convection. The model results indicate that when the negative anomalies associated with the ISO reach the Philippines, extratropical disturbances may be forced to form with the same spatial pattern as the initial stage of the positive EAP after 10 days through Rossby wave propagation. However, unlike the impact of convective anomalies over the Philippines on the triggering of the EAP, the influence of convective anomalies over the North Indian Ocean appears relatively limited.

The relationship between the BSISO and mid-latitude low-frequency disturbances was also exposed in Lu et al. (2007). They found that prior to the convection variability over the Philippines, a westward-traveling wave train would appear over the North Pacific. The above research work underlines the impact of extratropical variability on tropical convection, while this study emphasizes the influence of tropical convection on extratropical anomalies. These two works together indicate the tropical–extratropical interaction.

Due to the limitation of LBM, only the symmetric relationship between the ISO and the EAP could be identified in present study. However, since an asymmetric relationship between tropical convection and the EAP was suggested in Hsu and Lin (2007), i.e., the positive phase of the EAP appears to have a stronger tropical connection and the negative phase has a stronger extratropical connection, the asymmetry of triggering mechanism of the EAP should be considered as an important issue of future research.

Acknowledgments Authors thank Prof. M. Watanabe for his permitting the use of the LBM. This research was jointly supported by National Key Basic Research and Development Projects of China (2014CB953901), National Natural Science Foundation of China (41175076) and State Key Laboratory of Severe Weather opening project. R.W. acknowledges the support of National Natural Science Foundation of China Grants (41275081 and 41475081). J.W. acknowledges the support of the high-performance grid computing platform of Sun Yat-sen University.

References

- Black RX, Dole RM (1993) The dynamics of large-scale cyclone genesis over the North Pacific Ocean. *J Atmos Sci* 50:421–442
- Branstator G (1984) The relationship between the zonal mean flow and quasi-stationary waves in the mid troposphere. *J Atmos Sci* 41:2163–2178
- Branstator G (1990) Low-frequency patterns induced by stationary waves. *J Atmos Sci* 47:629–648
- Branstator G (1992) The maintenance of low-frequency atmospheric anomalies. *J Atmos Sci* 49:1924–1945
- Cai M, van den Dool HM (1994) Dynamical decomposition of low-frequency tendencies. *J Atmos Sci* 51:2086–2100
- Cassou C (2008) Intraseasonal interaction between the Madden–Julian oscillation and the North Atlantic oscillation. *Nature* 455:523–527
- Chen Z, Wen Z, Wu R, Zhao P, Cao J (2014) Influence of two types of El Niños on the East Asian climate during boreal summer: a numerical study. *Clim Dyn* 43:469–481. doi:10.1007/s00382-013-1943-1
- Choi K-S, Wu C-C, Cha E-J (2010) Change of tropical cyclone activity by Pacific–Japan teleconnection. *J Geophys Res* 115:1–13
- Dee DP et al (2011) The ERA-Interim reanalysis: configuration and performance of the data assimilation system. *Q J R Meteorol Soc* 137:533–597. doi:10.1002/qj.828
- Deng Y, Jiang T (2011) Intraseasonal modulation of the North Pacific storm track by tropical convection in boreal summer. *J Clim* 24:1122–1137. doi:10.1175/2010JCLI3676.1
- Duchon CE (1979) Lanczos filtering in one and 2 dimensions. *J Appl Meteorol* 18:1016–1022. doi:10.1175/1520-0450(1979)018<1016:LFIOA>2.0.CO;2
- Duncan B, Han W (2012) Influence of atmospheric intraseasonal oscillations on seasonal and interannual variability in the upper Indian Ocean. *J Geophys Res*. doi:10.1029/2012JC008190
- Egger J, Schilling H-D (1983) On the theory of the long-term variability of the atmosphere. *J Atmos Sci* 40:1073–1085
- Enomoto T, Hoskins BJ, Matsuda Y (2003) The formation mechanism of the Bonin high in August. *Q J R Meteorol Soc* 129:157–178. doi:10.1256/qj.01.211
- Feldstein S (1998) The growth and decay of low-frequency anomalies in a GCM. *J Atmos Sci* 55:415–428
- Feldstein S (2002) Fundamental mechanisms of the growth and decay of the PNA teleconnection pattern. *Q J R Meteorol Soc* 128:775–796
- Hendon HH, Wheeler MC, Zhang C (2007) Seasonal dependence of the MJO–ENSO relationship. *J Clim* 20:531–543
- Hoskins BJ, Karoly D (1981) The steady linear response of a spherical atmosphere to thermal and orographic forcing. *J Atmos Sci* 38:1179–1196
- Hsu P-C, Li T (2011a) Interactions between boreal summer intraseasonal oscillations and synoptic-scale disturbances over the western North Pacific. Part I: energetics diagnosis. *J Clim* 24:927–941. doi:10.1175/2010JCLI3833.1
- Hsu P-C, Li T (2011b) Interactions between boreal summer intraseasonal oscillations and synoptic-scale disturbances over the western North Pacific. Part II: apparent heat and moisture sources and eddy momentum transport. *J Clim* 24:942–961. doi:10.1175/2010JCLI3834.1
- Hsu H-H, Lin S-M (2007) Asymmetry of the tripole rainfall pattern during the East Asian summer. *J Clim* 20:4443–4458. doi:10.1175/JCLI4246.1
- Huang R (1992) The East Asia/Pacific pattern teleconnection of summer circulation and climate anomaly in East Asia. *Acta Meteorol Sin* 6:25–36
- Huang R, Li W (1987) Influence of the anomaly of heat source over the northwestern tropical Pacific for the subtropical high over East Asia. In: Proceedings of international conference on the general circulation of East Asia, April 10–15, 1987, Chengdu, China, pp 40–45
- Jin F-F, Pan L-L, Watanabe M (2006a) Dynamics of synoptic eddy and low-frequency flow feedback. Part I: a linear closure. *J Atmos Sci* 63:1677–1694
- Jin F-F, Pan L-L, Watanabe M (2006b) Dynamics of synoptic eddy and low-frequency flow feedback. Part II: a theory for low-frequency modes. *J Atmos Sci* 63:1695–1708
- Johnson NC, Feldstein S (2010) The continuum of North Pacific sea level pressure patterns: intraseasonal, interannual, and interdecadal variability. *J Clim* 23:851–867. doi:10.1175/2009JCLI3099.1
- Kang I-S (1990) Influence of zonal mean flow change on stationary wave fluctuations. *J Atmos Sci* 47:141–147
- Kawamura R, Ogasawara T (2006) On the role of typhoons in generating PJ teleconnection patterns over the western North Pacific in late summer. *SOLA* 2:37–40. doi:10.2151/sola.2006-010
- Kikuchi K, Wang B, Kajikawa Y (2012) Bimodal representation of the tropical intraseasonal oscillation. *Clim Dyn* 38:1989–2000. doi:10.1007/s00382-011-1159-1
- Kim J-S, Li C-YR, Zhou W (2012) Effects of the Pacific–Japan teleconnection pattern on tropical cyclone activity and extreme precipitation events over the Korean peninsula. *J Geophys Res*. doi:10.1029/2012JD017677
- Kosaka Y, Nakamura H (2006) Structure and dynamics of the summertime Pacific–Japan (PJ) teleconnection pattern. *Q J R Meteorol Soc* 132:2009–2030. doi:10.1256/qj.05.204
- Kosaka Y, Nakamura H (2008) A comparative study on the dynamics of the Pacific–Japan (PJ) teleconnection pattern based on reanalysis datasets. *SOLA* 4:9–12. doi:10.1251/sola.2008-003
- Kosaka Y, Nakamura H (2010) Mechanisms of meridional teleconnection observed between a summer monsoon system and a subtropical anticyclone. Part I: the Pacific–Japan pattern. *J Clim* 23:5085–5108. doi:10.1175/2010JCLI3413.1
- Lau N-C (1988) Variability of the observed midlatitude storm tracks in relation to low-frequency changes in the circulation pattern. *J Atmos Sci* 45:2718–2743
- Lau K-M, Weng H (2002) Recurrent teleconnection patterns linking summertime precipitation variability over East Asia and North America. *J Meteorol Soc Jpn* 80:1309–1324

- Li C-YR, Zhou W, Li T (2014) Influences of the Pacific–Japan teleconnection pattern on synoptic-scale variability in the western North Pacific. *J Clim* 27:140–154. doi:[10.1175/JCLI-D-13-00183.1](https://doi.org/10.1175/JCLI-D-13-00183.1)
- Lin H, Brunet G, Derome J (2009) An observed connection between the North Atlantic oscillation and the Madden–Julian oscillation. *J Clim* 22:364–380
- Lu R, Lin Z (2009) Role of subtropical precipitation anomalies in maintaining the summertime meridional teleconnection over the western North Pacific and East Asia. *J Clim* 22:2058–2072. doi:[10.1175/2008JCLI2444.1](https://doi.org/10.1175/2008JCLI2444.1)
- Lu R, Ding H, Ryu C-S, Lin Z, Dong H (2007) Midlatitude westward propagating disturbances preceding intraseasonal oscillations of convection over the subtropical western North Pacific during summer. *Geophys Res Lett* 34:L21702. doi:[10.1029/2007GL031277](https://doi.org/10.1029/2007GL031277)
- Madden RA, Julian PR (1971) Detection of a 40–50 day oscillation in the zonal wind in the tropical Pacific. *J Atmos Sci* 28:702–708
- Madden RA, Julian PR (1972) Description of global-scale circulation cells in the tropics with a 40–50 day period. *J Atmos Sci* 29:1109–1123
- Madden RA, Julian PR (1994) Observations of the 40–50-day tropical oscillation—a review. *Mon Weather Rev* 122:814–837
- McPhaden MJ (1999) Genesis and evolution of the 1997–98 El Niño. *Science* 283:950–954
- McPhaden MJ (2004) Evolution of the 2002/03 El Niño. *Bull Am Meteor Soc* 85:677–695
- McPhaden MJ (2008) Evolution of the 2006–07 El Niño: the role of intraseasonal to interannual time scale dynamics. *Adv Geosci* 14:219–230
- Mori M, Watanabe M (2008) The growth and triggering mechanisms of the PNA: a MJO–PNA coherence. *J Meteor Soc Jpn* 86:213–236
- Nigam S, Lindzen RS (1989) The sensitivity of stationary waves to variations in the basic state zonal flow. *J Atmos Sci* 46:1746–1768
- Nitta T (1987) Convective activities in the tropical western Pacific and their impact on the northern hemisphere summer circulation. *J Meteor Soc Jpn* 65:373–390
- North GR, Bell TL, Cahalan RF, Moeng FJ (1982) Sampling errors in the estimation of empirical orthogonal functions. *Mon Weather Rev* 110:699–706
- Rao SA, Luo J-J, Behera SK, Yamagata T (2008) Generation and termination of Indian Ocean dipole events in 2003, 2006, 2007. *Clim Dyn* 33:751–767
- Schubert SD, Park C-K (1991) Low-frequency intraseasonal tropical–extratropical interactions. *J Atmos Sci* 48:629–650
- Seiki A, Takayabu YN (2007) Westerly wind bursts and their relationship with intraseasonal variations and ENSO. Part II: energetics over the western and central Pacific. *Mon Weather Rev* 135:3346–3361
- Simmons AJ, Wallace JM, Branstator G (1983) Barotropic wave propagation and instability and atmospheric teleconnection patterns. *J Atmos Sci* 40:1363–1392
- Straub KH, Kiladis GN (2003) Interactions between the boreal summer intraseasonal oscillation and higher frequency tropical wave activity. *J Atmos Sci* 131:945–960
- Takaya K, Nakamura H (2001) A formulation of a phase-independent wave-activity flux for stationary and migratory quasigeostrophic eddies on a zonally varying basic flow. *J Atmos Sci* 58:608–627
- Thompson DWJ, Wallace JM (2000) Annular modes in the extratropical circulation. Part I: month-to-month variability. *J Clim* 13:1000–1016
- Ting M, Lau N-C (1993) A diagnostic and modeling study of the monthly mean wintertime anomalies appearing in an 100-year GCM experiment. *J Atmos Sci* 50:2845–2867
- Watanabe M, Kimoto M (2000) Atmosphere–ocean thermal coupling in the North Atlantic: a positive feedback. *Q J R Meteorol Soc* 126:3343–3369. doi:[10.1002/qj.49712657017](https://doi.org/10.1002/qj.49712657017)
- Watanabe M, Kimoto M (2001) Corrigendum. *Q J R Meteorol Soc* 127:733–734
- Wheeler MC, Hendon HH (2004) An all-season real-time multivariate MJO index: development of an index for monitoring and prediction. *Mon Weather Rev* 122:1917–1932
- Wu J, Xu X, Jin F-F, Guo P (2013) Research of the intraseasonal evolution of the East Asia Pacific pattern and the maintenance mechanism. *Acta Meteor Sin* 71:476–491. doi:[10.11676/qxxb2013.038](https://doi.org/10.11676/qxxb2013.038) (in Chinese)
- Yamada K, Kawamura R (2007) Dynamical link between typhoon activity and the PJ teleconnection pattern from early summer to autumn as revealed by the JRA-25 reanalysis. *SOLA* 3:65–68. doi:[10.2151/sola.2007-017](https://doi.org/10.2151/sola.2007-017)
- Yoo C, Lee S, Feldstein S (2012) Mechanisms of arctic surface air temperature change in response to the Madden–Julian oscillation. *J Clim* 25:5777–5790
- Zhang C (2013) Madden–Julian oscillation: bridging weather and climate. *Bull Am Meteor Soc* 94:1849–1870. doi:[10.1175/BAMS-D-12-00026.1](https://doi.org/10.1175/BAMS-D-12-00026.1)
- Zhang C, Gottschalck J (2002) SST anomalies of ENSO and the Madden–Julian oscillation in the equatorial Pacific. *J Clim* 15:2429–2445